

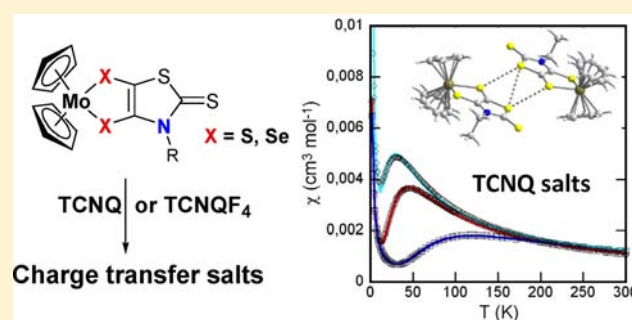
Variable Magnetic Interactions between $S = 1/2$ Cation Radical Salts of Functionalizable Electron-Rich Dithiolene and Diselenolene Cp_2Mo Complexes

Talia Bsaibess, Michel Guerro, Yann Le Gal, Daad Sarraf, Nathalie Bellec, Marc Fourmigué, Frédéric Barrière, Vincent Dorcet, Thierry Guizouarn, Thierry Roisnel, and Dominique Lorcy*

Institut des Sciences Chimiques de Rennes, UMR 6226 CNRS-Université de Rennes 1, Campus de Beaulieu, Bât 10A, 35042 Rennes cedex, France

Supporting Information

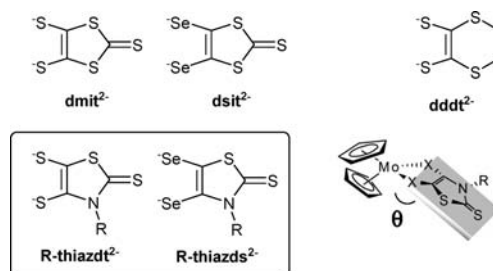
ABSTRACT: A series of Cp_2Mo (dithiolene) and Cp_2Mo (diselenolene) complexes containing N-alkyl-1,3-thiazoline-2-thione-4,5-dithiolate ligand (R-thiazdt, R = Me, Et, CH_2CH_2OH) and N-alkyl-1,3-thiazoline-2-thione-4,5-diselenolate ligand (R-thiazds, R = Me, Et) have been synthesized. These heteroleptic molybdenum complexes have been characterized by electrochemistry, spectroelectrochemistry, and single crystal X-ray diffraction. They act as very good electron donor complexes with a first oxidation potential 200 mV lower than in the prototypical Cp_2Mo (dmit) complex and exhibit almost planar MoS_2C_2 (or $MoSe_2C_2$) metallacycles. All five complexes formed charge transfer salts with a weak (TCNQ) and a strong acceptor (TCNQF₄), affording ten different charge-transfer salts, all with 1:1 stoichiometry. Crystal structure determinations show that the S/Se substitution in the metallacycle systematically affords isostructural salts, while the Cp_2Mo (R-thiazdt) complexes with R equals ethyl or CH_2CH_2OH can adopt different structures, depending on the involvement of the hydroxyl group into intra- or intermolecular hydrogen bonding interactions. Magnetic susceptibility data of the salts are correlated with their structural organization, demonstrating that a face-to-face organization of the Me-thiazdt (or Me-thiazds) ligand favors a strong antiferromagnetic interaction, while the bulkier R = Et or R = CH_2CH_2OH substituents can completely suppress such intermolecular interactions, with the added contribution of hydrogen bonding to the solid state organization.



INTRODUCTION

Mixed bis(cyclopentadienyl) dithiolene molybdenum complexes, formulated as Cp_2Mo (dithiolene), are electron rich, d^2 complexes, which can be oxidized reversibly into cation radical species. The ease of oxidation has led recently to their incorporation as donor component into a donor–acceptor array leading to the first example of a charge separated dyad involving a Cp_2Mo (dithiolene) complex.¹ These complexes have also been used as model compounds for the active site of the so-called molybdenum cofactor ($MoCo$)^{2–4} as well as for the elaboration of crystalline, magnetic molecular materials.^{5,6} Indeed, depending on the solid state organization of these cation radical species and the strength and directionality of intermolecular interactions, different magnetic behaviors have been observed in the solid state, from singlet–triplet dimers to spin chains,^{7,8} spin ladders,^{9,10} or antiferromagnetic ground state.^{8,9} Up to now, these structural and magnetic studies were essentially restricted to only three different dithiolene (or diselenolene) ligands (Chart 1), namely $dmit^{2-}$ (2-thioxo-1,3-dithiole-4,5-dithiolate), its selenolate analog $dsit^{2-}$ (2-thioxo-1,3-dithiole-4,5-diselenolate), and the more electron-rich ddd^{2-} (5,6-dihydro-1,4-dithiine-2,3-dithiolate).⁷ Another attractive feature of these complexes is the flexibility of the MoS_2C_2

Chart 1



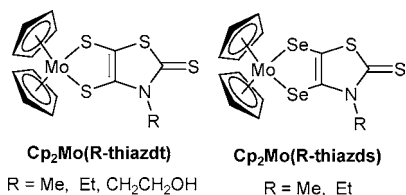
metallacycle, with folding angle (θ) along the S...S hinge (Chart 1) varying between 0 and 50°, depending on the nature of the dithiolene ligand, and the electron count of the complexes.⁵ Indeed, while d^2 Cp_2Mo (dithiolene) exhibits a close to zero θ value, the cationic $[Cp_2Mo(dithiolene)]^+$ complexes, formally d^1 , show pronounced folding angles, from 0 to 35°. This is associated with a variable delocalization of the spin density, essentially on the

Received: November 27, 2012

Published: January 29, 2013

dithiolene moiety for unfolded complexes ($0 \leq \theta \leq 10\text{--}15^\circ$) and more delocalized on the Cp_2M moiety in folded ones. Since intermolecular interactions in the solid state are mediated by the direct overlap of the dithiolene moieties, it was shown that the strongest interactions were indeed associated with the less distorted complexes.

In order to strengthen the magnetic interactions in the solid state in such systems, it is therefore advisable to investigate dithiolene ligands that are easier to oxidize than the dmit/dsit or ddt ones, to possibly concentrate the spin density essentially on the dithiolene ligand into weakly folded complexes. We recently reported the synthesis of a novel dithiolene (and diselenolene) ligand incorporating a R–N group within a thiazoline ring, noted R-thiazdt²⁻ for N-alkyl-1,3-thiazoline-2-thione-4,5-dithiolate and R-thiazds²⁻ for the corresponding diselenolene, N-alkyl-1,3-thiazoline-2-thione-4,5-diselenolate. Investigations of the homoleptic $[\text{M}(\text{R-thiazdt})_2]^{n-}$ (M = Zn,¹¹ Ni,¹² Pd and Au)¹³ metal complexes as well as the heteroleptic Cp_2Ti ¹⁴ and Pt(diimine)¹⁵ complexes showed that these ligands are particularly electron-rich ligands, when compared with their all-sulfur analogues such as dmit²⁻. Moreover, the thiazoline ring offers the possibility of numerous structural modifications through the nitrogen substituent. Therefore, we decided to investigate the corresponding heteroleptic Cp_2Mo complexes of these original dithiolene and diselenolene ligands, formulated as $\text{Cp}_2\text{Mo}(\text{R-thiazdt})$ or $\text{Cp}_2\text{Mo}(\text{R-thiazds})$, in order to compare the properties of these hitherto unknown derivatives with their sulfur analogues $\text{Cp}_2\text{Mo}(\text{dmit})$ and $\text{Cp}_2\text{Mo}(\text{dsit})$, to determine the influence of the thiazole skeleton on their electrochemical properties and to investigate the structural and magnetic properties of their cation radical salts.

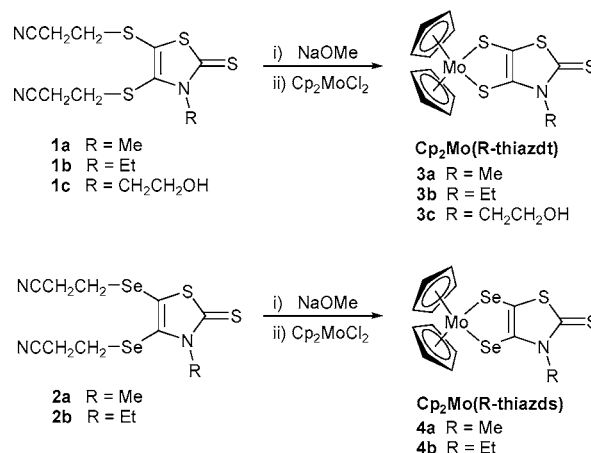


In this paper, we present the synthesis of five Cp_2Mo -(dithiolene) or Cp_2Mo -(diselenolene) complexes with different R substituents on the nitrogen atom of the thiazoline ring R = Me, Et, or $\text{CH}_2\text{CH}_2\text{OH}$. The choice of these substituents was determined by two criteria: i) an anticipated similar effect on the overall electron donating properties of the complexes and ii) a notably different steric hindrance, in order to modulate the intermolecular interactions in the solid state or create, thanks to hydrogen bonding, intermolecular interactions. The low oxidation potential of these complexes allowed the formation of charge transfer salts with both TCNQ and TCNQF_4 as electron acceptors. These salts have been fully characterized by X-ray structure determinations and static and dynamic magnetic studies. Depending on the nature of the R substituent carried out by the nitrogen of the heterocyclic ring (R = Me, Et, or $\text{CH}_2\text{CH}_2\text{OH}$), different solid state organizations and magnetic behaviors were found, all characterized indeed by strong antiferromagnetic interactions in the solid state.

RESULTS AND DISCUSSION

Synthesis and Characterization of Dithiolene and Diselenolene Cp_2Mo Complexes. *Syntheses.* The chemical approach used for the synthesis of the target molecules is described in Scheme 1. The starting point is the organic

Scheme 1



dithiolate or diselenolate hidden form of the ligand, the N-alkyl-bis(cyanoethylthio)-1,3-thiazoline-2-thione **1a–c** and N-alkyl-bis(cyanoethylseleno)-1,3-thiazoline-2-thione **2a–b**, where the two thiolate and selenolate functions are protected by cyanoethyl groups.^{11–14} Deprotection of the dithiolate and diselenolate ligands was performed in basic medium using NaOMe. Addition of Cp_2MoCl_2 afforded the dithiolene complexes **3a–c** and the diselenolene complexes **4a–b** in good yields (63–79%). The complexes are air stable, dark red crystalline materials, soluble in common organic solvents.

Electrochemical Properties. The redox behavior of $\text{Cp}_2\text{Mo}(\text{R-thiazdt})$ **3a–c** and $\text{Cp}_2\text{Mo}(\text{R-thiazds})$ **4a–b** was explored by cyclic voltammetry in dichloromethane solution with 0.1 M nBu_4NPF_6 as supporting electrolyte. All these heteroleptic complexes exhibit two reversible mono-electronic oxidation processes. These oxidation processes are attributed to the oxidation of the neutral complex to the cationic radical and dicationic species. The data are collected in Table 1 and are given in V vs

Table 1. Redox Potentials of $\text{Cp}_2\text{Mo}(\text{R-thiazdt})$ **3a–c and $\text{Cp}_2\text{Mo}(\text{R-thiazds})$ **4a–b** (E in V vs SCE), $\Delta E = E^2_{1/2} - E^1_{1/2}$**

	$E^1_{1/2}$	$E^2_{1/2}$	ΔE (mV)
Dithiolene Complexes			
$\text{Cp}_2\text{Mo}(\text{Me-thiazdt})$ 3a	0.19	0.80	610
$\text{Cp}_2\text{Mo}(\text{Et-thiazdt})$ 3b	0.19	0.81	620
$\text{Cp}_2\text{Mo}(\text{EtOH-thiazdt})$ 3c	0.20	0.80	600
$\text{Cp}_2\text{Mo}(\text{dmit})$	0.39	1.03	640
Diselenolene Complexes			
$\text{Cp}_2\text{Mo}(\text{Me-thiazds})$ 4a	0.26	0.82	560
$\text{Cp}_2\text{Mo}(\text{Et-thiazds})$ 4b	0.26	0.82	560
$\text{Cp}_2\text{Mo}(\text{dsit})$	0.42	1.03	610

SCE together with the redox potentials of the analogous dithiolene $\text{Cp}_2\text{Mo}(\text{dmit})$ and diselenolene $\text{Cp}_2\text{Mo}(\text{dsit})$ with a dithiole backbone which were re-examined in the same experimental conditions for comparison. As expected, there is no difference of redox potentials when the methyl group on the nitrogen atom in **3a** or **4a** is replaced by an ethyl group or hydroxyethyl one. We observe that the first oxidation process of the dithiolene derivatives **3a–c** occurs at a lower potential (–70 mV) than that of the diselenolene complexes **4a–b**, while the second oxidation occurs at the same potential.

A similar shift is observed for the dithiole analogues (dmit vs dsit). The most important point is that in both dithiolene and

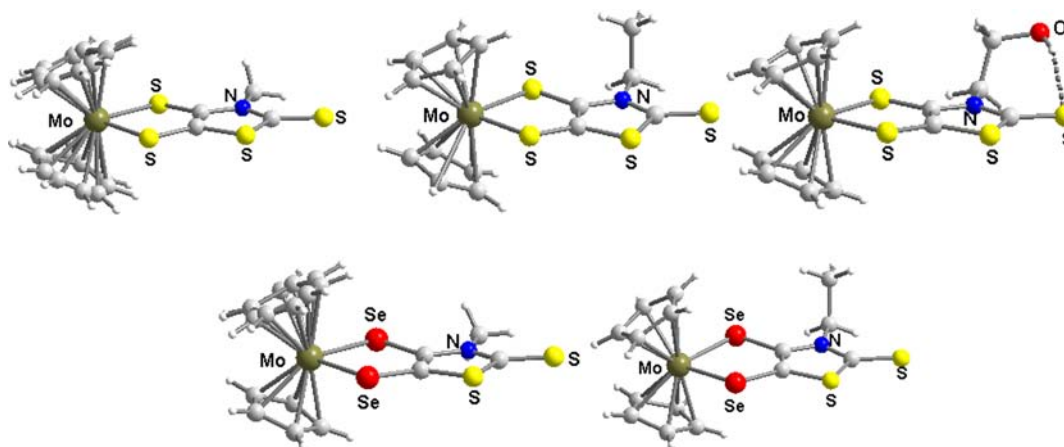


Figure 1. Molecular structure of $\text{Cp}_2\text{Mo}(\text{R-thiazdt})$ $\text{R} = \text{Me}$ **3a**, $\text{R} = \text{Et}$ **3b**, $\text{R} = \text{CH}_2\text{CH}_2\text{OH}$ **3c**, $\text{Cp}_2\text{Mo}(\text{Me-thiazds})$ **4a**, and $\text{Cp}_2\text{Mo}(\text{Et-thiazds})$ **4b**.

Table 2. Significant Bond Lengths [\AA] and Angles [$^\circ$] within the MoX_2C_2 ($\text{X} = \text{S}, \text{Se}$) Metallacycle in **3a–c** and **4a–b** and Their TCNQ and TCNQF₄ Salts^a

compound	Mo–X	X–C	C=C	X–Mo–X	θ
$\text{Cp}_2\text{Mo}(\text{Me-thiazdt})$ 3a	2.478(1), 2.465(1)	1.742(2), 1.741(2)	1.347(3)	84.78(2)	2.79(6)
[3a][TCNQ]	2.476(1), 2.477(1)	1.699(3), 1.724(3)	1.380(4)	84.01(3)	4.17(7)
[3a][TCNQF ₄]	2.463(2), 2.466(1)	1.696(2), 1.706(3)	1.388(3)	83.37(2)	19.77(5)
$\text{Cp}_2\text{Mo}(\text{Et-thiazdt})$ 3b	2.469(1), 2.485(1)	1.743(2), 1.756(2)	1.346(3)	84.40(2)	6.04(5)
[3b][TCNQ]	2.456(5), 2.475(8)	1.699(6), 1.714(4)	1.401(5)	84.24(2)	14.04(5)
[3b][TCNQF ₄]	2.461(3), 2.485(2)	1.701(3), 1.714(3)	1.395(4)	83.48(2)	17.22(5)
$\text{Cp}_2\text{Mo}(\text{EtOH-thiazdt})$ 3c	2.474(1), 2.467(1)	1.748(2), 1.739(2)	1.349(3)	84.64(2)	2.85(5)
[3c][TCNQ]	2.445(1), 2.470(2)	1.695(3), 1.707(3)	1.393(4)	84.19(3)	15.89(7)
[3c][TCNQF ₄]	2.454(1), 2.463(1)	1.694(3), 1.700(2)	1.392(3)	83.91(2)	5.50(5)
$\text{Cp}_2\text{Mo}(\text{dmit})$ ⁹	2.457(3)	1.745(9)	1.357(12)	83.9(1)	5.2(2)
[$\text{Cp}_2\text{Mo}(\text{dmit})$][TCNQF ₄] ¹⁰	2.444(4), 2.448(1)	1.684(13), 1.681(14)	1.43(2)	83.12(13)	10.2(1)
$\text{Cp}_2\text{Mo}(\text{Me-thiazds})$ 4a	2.588(5), 2.609(4)	1.893(4), 1.897(3)	1.344(3)	85.38(1)	3.84(5)
[4a][TCNQ]	2.596(1), 2.592(1)	1.850(3), 1.876(3)	1.374(4)	84.98(1)	0.90(5)
[4a][TCNQF ₄]	2.583(0), 2.590(1)	1.855(3), 1.860(3)	1.381(3)	84.26(1)	25.53(6)
$\text{Cp}_2\text{Mo}(\text{Et-thiazds})$ 4b	2.598(1), 2.603(2)	1.904(5), 1.906(5)	1.344(7)	85.27(2)	8.26(9)
[4b][TCNQ]	2.561(2), 2.583(3)	1.846(4), 1.858(5)	1.386(6)	85.01(2)	18.29(7)
[4b][TCNQF ₄]	2.461(3), 2.485(2)	1.701(3), 1.714(3)	1.395(4)	83.48(2)	18.25(8)
[$\text{Cp}_2\text{Mo}(\text{dsit})$][TCNQF ₄] ¹⁰	2.559(2), 2.563(2)	1.86(1), 1.86(1)	1.38(2)	83.68(5)	27.90(6)

^aSee Chart 1 for the definition of θ .

diselenolene series, the first oxidation of our thiazole derivatives **3a–c** and **4a–b** is observed at a significantly more cathodic potential (160–200 mV) than the oxidation of the corresponding dithiole derivatives $\text{Cp}_2\text{Mo}(\text{dmit})$ and $\text{Cp}_2\text{Mo}(\text{dsit})$.

X-ray Structure Analysis. Crystals of the heteroleptic neutral dithiolenes complexes **3a**, **3b**, and **3c** together with those of the diselenolene complexes **4a** and **4b** were obtained after recrystallization in chloroform. The molecular structures of **3a–c** and **4a–b** are given in Figure 1. Geometrical characteristics of the complexes are collected in Table 2 together with those of the dithiole dithiolenes $\text{Cp}_2\text{Mo}(\text{dmit})$ analogue.⁹ As shown in Figure 1, all these heteroleptic complexes exhibit the same structural trends: the thiazole cores are planar, and the metallacycles are weakly folded along the S...S or the Se...Se axis with an angle lying in the range 3–8°. The ethyl and hydroxyethyl substituents on the nitrogen of the thiazole ring in $\text{Cp}_2\text{Mo}(\text{R-thiazdt})$ **3b** and **3c** point out of the plane. Moreover, for the complex **3c** we can notice an intramolecular O–H...S hydrogen bonding between the hydroxyl and the thione of the thiazole core with H...S distance of 2.058(33) Å, leading to a seven membered ring.¹⁶ For all

complexes **3a–c** and **4a,b**, due to the asymmetrical character of the dithiolenes and diselenolene ligands, two different Mo–S and S–C bond lengths within each metallacycle are observed.¹⁷ The ligand bite angles and the Mo–S and S–C distances are comparable to those observed in the corresponding $\text{Cp}_2\text{Mo}(\text{dmit})$.⁹ Therefore the thiazole backbone has no influence on the overall geometry of these heteroleptic complexes. Among all these complexes, only one exhibits short intermolecular S...Se and the Se...Se contacts as depicted in Figure 2.

UV–vis–NIR spectroelectrochemical investigations were carried out on the complex $\text{Cp}_2\text{Mo}(\text{Me-thiazdt})$ **3a** in order to get more insight into the formation of the various oxidized species. The neutral complexes exhibit absorption bands in the visible range at $\lambda_{\text{max}} = 261–269$ nm ($\epsilon = 11000–19800$ L mol^{−1} cm^{−1}) and 388–400 nm ($\epsilon = 6300–10190$ L mol^{−1} cm^{−1}), close to that observed for other Cp_2Mo dithiolenes complexes.^{18,17} Upon gradual oxidation to the mono-oxidized species **3a^{•+}** (Figure 3, top), four new absorption bands centered at $\lambda_{\text{max}} = 324, 468, 643,$ and 1054 nm grow, the latter being a broad absorption band, concomitant with the decrease of the band centered at 396 nm.

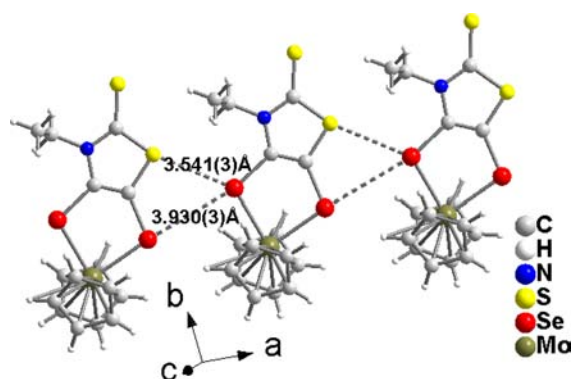


Figure 2. View of the short S...Se and Se...Se contacts in Cp_2Mo -(Et-thiazds) **4b**.

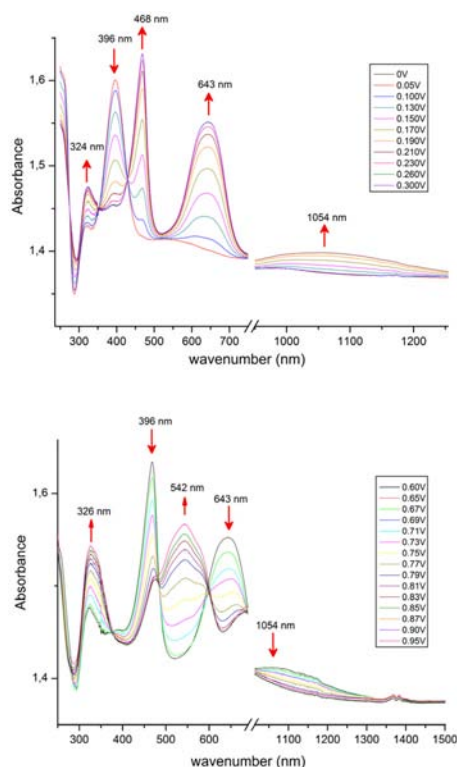


Figure 3. UV-vis-NIR monitoring of the first (top) and the second (bottom) electrochemical oxidation of **3a** in CH_2Cl_2 -[NBu₄][PF₆] 0.2 M.

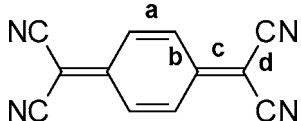
Upon gradual oxidation to the dioxidized species 3^{2+} (Figure 3, bottom), new absorption bands centered at $\lambda_{\text{max}} = 542$ nm grow, attributed to the signature of the dicationic species, together with the increase of the band centered at 326 nm while the absorption bands centered at 468, 643, and 1054 nm decrease.

Charge Transfer Salts with TCNQ and TCNQF₄. The low oxidation potentials (Table 1) of $\text{Cp}_2\text{Mo}(\text{R-thiazdt})$ **3a–c** and $\text{Cp}_2\text{Mo}(\text{R-thiazds})$ **4a–b** complexes open the possibility to form charge transfer salts with two organic acceptors, TCNQ which is reduced at 0.18 V vs SCE and TCNQF₄ which is a stronger electron acceptor as it reduces at 0.53 V vs SCE. The salts were obtained by mixing hot solutions of the molybdenum complex in CH_2Cl_2 with a solution of TCNQ or TCNQF₄ in CH_3CN . Deep violet crystals were obtained, and crystal structure determinations reveal in all cases a 1:1 stoichiometry with one Mo complex for one acceptor. The degree of charge transfer

between donor and acceptor molecules can be inferred from analysis of the bond lengths within the TCNQ and the TCNQF₄ skeletons (Table 3). Concerning the five TCNQ complexes, this can be done by using the empirical formula of Kistenmacher (Table 3).¹⁹ Accordingly, we found a value close to -1 for all five salts except for the Me-thiazdt and Me-thiazds complexes **3a** and **4a** with apparently a lower degree of charge transfer. Note that TCNQ, even if it is a weak electron acceptor, can oxidize all five $\text{Cp}_2\text{Mo}(\text{R-thiazdt})$ and $\text{Cp}_2\text{Mo}(\text{R-thiazds})$ complexes reported here, in sharp contrast with the sulfur analogues $\text{Cp}_2\text{Mo}(\text{dmit})$ and $\text{Cp}_2\text{Mo}(\text{dsit})$ which were not oxidized by TCNQ.¹⁰ The reduction of TCNQ into TCNQ anion radical within these salts is also supported by the nitrile stretching absorption band in the FTIR spectra of each salt (Table 3). The nitrile vibration band observed for neutral TCNQ is found at $\nu_{\text{CN}} = 2227$ cm^{-1} , while for all complexes it was found at a lower energy value which is close to that reported for TCNQ⁻¹ ($\nu_{\text{CN}} = 2185$ cm^{-1}) in its Na^+TCNQ^- salt.²⁰ The isolation of salts with full charge transfer with TCNQ, despite slightly unfavorable redox potentials, finds its origin in the Coulombic stabilization of charge species provided by the crystal formation.²¹ Considering now the TCNQF₄ salts (Table 2), similar variations of the intramolecular bond distances occur upon reduction, and the quinoid structure of neutral TCNQF₄ evolves toward an aromatic structure through a shortening of the *b* bonds and a concomitant lengthening of the *a* bonds. Actually these bond length modifications with the charge are less pronounced than in the case of the TCNQ especially on the *c* and *d* bonds. The reduction of the TCNQF₄ into the anion radical is also supported by the nitrile stretching absorption band in the FTIR spectra of each complex. The nitrile vibration band observed for neutral TCNQF₄ is located at $\nu_{\text{CN}} = 2225$ cm^{-1} , while for all the complexes it was found at a lower energy value which is close to the one observed for TCNQF₄⁻¹ ($\nu_{\text{CN}} = 2195$ and 2179 cm^{-1}) in its $[\text{Cp}_2\text{Fe}][\text{TCNQF}_4]^-$ salt.²²

The donor skeleton itself is also subject to bond length and bond angle modifications upon oxidation. As the neutral complexes have been also characterized by crystal X-ray diffraction study, it is possible to evaluate the geometrical modifications occurring between the neutral and the oxidized state of $[\text{Cp}_2\text{Mo}(\text{R-thiazdt})]$ and $[\text{Cp}_2\text{Mo}(\text{R-thiazds})]$ (Table 2). A common characteristic within all these complexes in the oxidized state concerns the modification of the bond lengths within the metallacycle ring. For instance, the S–C or Se–C bonds are systematically shortened, while the C=C bonds are lengthened, indicating that the oxidation process strongly affects the dithiolene moiety which adopts indeed a more dithio (or diseleno) ketonic structure.

The folding angles θ along the S...S and the Se...Se axis observed for all the $\text{Cp}_2\text{Mo}(\text{R-thiazdt})^{\bullet+}$ and $\text{Cp}_2\text{Mo}(\text{R-thiazds})^{\bullet+}$ cation radical species vary extensively, in the range 1–25°. The apparently less oxidized TCNQ salts with **3a** and **4a** (see above) exhibit unfolded structures with θ angles of 4.2 and 0.9°. However, in $[\text{3c}][\text{TCNQF}_4]$ where the full charge transfer is unambiguous, a small 5.5° folding angle is also found. Therefore no correlation between the degree of charge transfer and the folding angle can be established here in the solid state, an illustration of the flexibility of the metallacycles in such complexes. Indeed it has been shown that oxidized species usually show a more pronounced folding angle than the neutral species. Another trend is that the same oxidized species, depending on the radical anion, can be more or less folded. This behavior is reminiscent of that found with the analogous $\text{Cp}_2\text{Mo}(\text{dmit})^{\bullet+}$ species where highly variable folding

Table 3. Significant Intramolecular Averaged Bond Lengths (Å) in TCNQ and TCNQF₄ Salts^a


compound	<i>a</i> (Å)	<i>b</i> (Å)	<i>c</i> (Å)	<i>d</i> (Å)	ρ	ν_{CN} (cm ⁻¹)	ref
TCNQ ⁰	1.346	1.448	1.374	1.441	-0.02	2227	23, 24
[Na ⁺][TCNQ ^{•-}]	1.354	1.427	1.419	1.420	-0.94	2185	25, 16
[3a][TCNQ]	1.3545	1.435	1.4055	1.427	-0.63	2186	this work
[3b][TCNQ]	1.3655	1.428	1.422	1.425	-0.94	2180	this work
[3c][TCNQ]	1.362	1.4245	1.4185	1.425	-0.91	2181	this work
[4a][TCNQ]	1.356	1.4345	1.3975	1.426	-0.52	2188	this work
[4b][TCNQ]	1.351	1.425	1.418	1.420	-0.93	2175	this work
TCNQF ₄ ⁰	1.344	1.433	1.388	1.4345	0	2215, 2230	26, 27
Cp ₂ Fe ⁺ TCNQF ₄ ^{•-}	1.360	1.420	1.429	1.435	-1	2179, 2195	17, 20
[3a][TCNQF ₄]	1.358	1.41525	1.413	1.42375	≈-1	2175, 2188	this work
[3b][TCNQF ₄]	1.3575	1.421	1.4155	1.4352	≈-1	2178, 2196	this work
[3c][TCNQF ₄]	1.349	1.4222	1.406	1.4272	≈-1	2175, 2194	this work
[4a][TCNQF ₄]	1.359	1.4185	1.413	1.4272	≈-1	2174, 2191	this work
[4b][TCNQF ₄]	1.3555	1.4195	1.4175	1.42625	≈-1	2175, 2191	this work

^aThe charge (ρ) in TCNQ compounds is calculated according to the Kistenmacher formula which reads as $\rho = A(c/(b + d)) + B$ with $A = -41.667$ and $B = 19.833$. The charge (ρ) in TCNQF₄ salts is estimated from the bond length comparison.

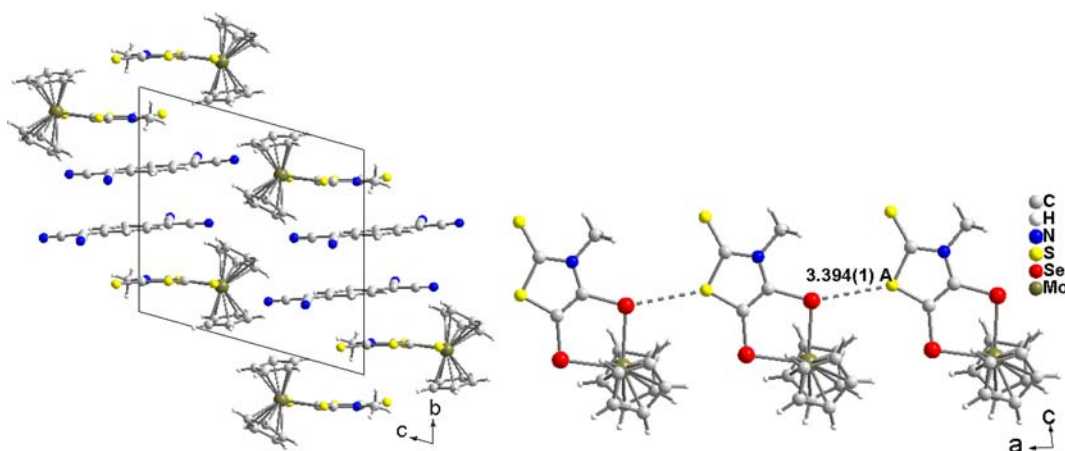


Figure 4. View of the unit cell of [3a][TCNQ] along the *bc* plane (left) and S...S interactions along the *a* axis for [4a][TCNQ] (right).

angles (0–35°) were found depending on the nature of the counterion in various salts.⁴

In the solid state, different structural organisations depending on the substituent carried out by the nitrogen of the thiazole ring can be observed, while the S/Se substitution systematically affords isostructural compounds. For instance, the TCNQ salts of the N-Me derivatives 3a and 4a, namely [3a][TCNQ] and [4a][TCNQ], are isostructural, and they crystallize in the triclinic system space group $P\bar{1}$, with cation and anion in general position (Figure 4). The acceptor molecules form isolated dimers with a bond-over-ring longitudinal slip. The intradimer plane to plane distance amounts to 3.25–3.26 Å in both salts, to be compared with 3.19 Å found between TCNQ in TTF·TCNQ for example.²⁸ The donors form also dimers with a head to tail organization, the thiazole ring of one complex facing the thiazole ring of another complex. The shortest intradimer S...S distances between the S atom of the thiazole ring and the exocyclic S atom amount to 3.654(3) and 3.650(2) Å in [3a][TCNQ] and [4a][TCNQ], respectively. Short S...S and S...Se contacts can also be observed along the *a* axis between the neighboring dimers being equal to 3.446(2) Å in

[3a][TCNQ] and to 3.394(1) Å in [4a][TCNQ] (Figure 4). Note also the presence of face-to-face Cp...Cp contacts between neighboring cations at the center of the unit cell.²⁹

This structural organization lets us infer that the magnetic properties of these two salts will be dominated by the contribution of the organometallic cations as the short plane-to-plane distances within the TCNQ dimers might lead to a pairing of the two radical anion species in the bonding combination of the two TCNQ LUMOs. Temperature dependence of the magnetic susceptibility of the two salts show an essentially diamagnetic behavior with a Curie tail accounting for 0.7 and 3.6% $S = 1/2$ magnetic defaults in [3a][TCNQ] and [4a][TCNQ], respectively. This demonstrates that, not only within the TCNQ dyads but also within the 3a (or 4a) inversion centered face-to-face dyads, the cation radical species are also strongly associated. In order to check this assumption, the $\beta_{\text{HOMO-HOMO}}$ interaction energy within the dicationic dyads was calculated, affording β values of 0.22 and 0.27 eV in [3a][TCNQ] and [4a][TCNQ], respectively, and demonstrating unambiguously the strong overlap taking place between the 3a^{•+} or 4a^{•+} radical cations through the short S...S intermolecular contacts.

As mentioned above, the TCNQF₄ salts with N-Me derivatives **3a** and **4a** are also isostructural. They crystallize in the monoclinic system, space group *C2/c* with cation and anion in general position (Figure 5). The TCNQF₄ form strongly di-

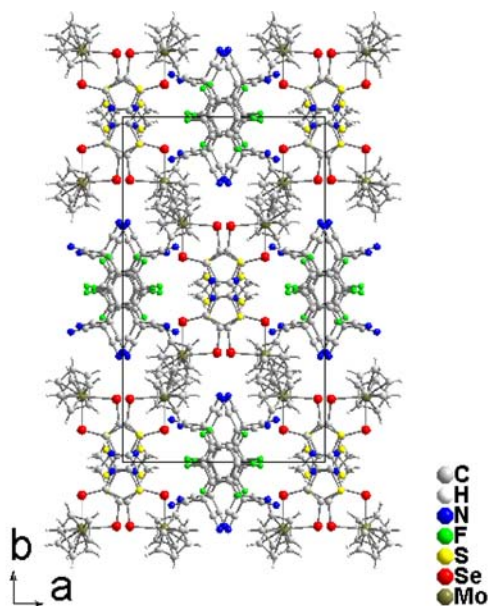


Figure 5. Projection view along the *c* axis of the unit cell of [4a][TCNQF₄] (top), TCNQF₄ intradimer overlap (bottom left), and TCNQF₄ interdimer overlap (bottom right).

merized chains running along the *c* axis, with a lateral slip observed between the two neighboring molecules within the inversion-centered dimers, and a rotation of the molecular long axis of $\approx 60^\circ$ between the dimers through the 2-fold axis (Figure 5). The plane-to-plane distance within the TCNQF₄ dimers is very short, 3.07–3.08 Å, indicating a strong overlap interaction between the TCNQF₄ LUMOs. The organometallic cations form also dimerized chains running along the *c* axis. The inversion centered dyads overlap only through the outer thiazole-2-thione moieties, with long S...S intermolecular contacts, 3.940(2) Å and 3.991(2) Å in [3a][TCNQF₄] and [4a][TCNQF₄], respectively. On the other hand, face-to-face interdimer interactions between radical cations related through the 2-fold axis involves the metallacycle chalcogen atoms, with very short intermolecular S...S [3.339(2) Å] and Se...Se [3.265(1) Å] contacts (Figure 6).

The temperature dependence of the magnetic susceptibility of the two salts shows an essentially diamagnetic behavior with a Curie tail accounting for 3.2 and 2.5% $S = 1/2$ magnetic defaults in [3a][TCNQF₄] and [4a][TCNQF₄], respectively, demonstrating that here again an efficient overlap interaction takes place, not only between TCNQF₄^{•-} radical anions but also between 3a^{•+} and 4a^{•+} radical cations. Calculations of the $\beta_{\text{HOMO-HOMO}}$ interaction energies within the cation radical

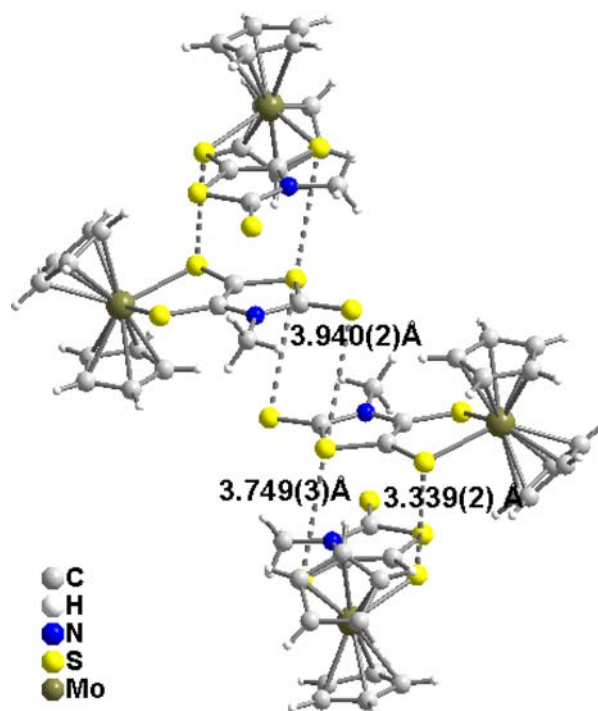


Figure 6. S...S interactions within [3a][TCNQF₄].

chains confirm that the strongest interactions are indeed between those cations related by the 2-fold axis, with large β values of 0.41 and 0.69 eV in [3a][TCNQF₄] and [4a][TCNQF₄], respectively, while a weaker overlap is indeed confirmed in the inversion-centered dyads, with β values of 0.17 and 0.10 eV.

The TCNQ salts of the N-Et derivatives **3b** and **4b**, i.e. [3b][TCNQ] and [4b][TCNQ] are also isostructural, together with that obtained with the dithiolenone complex **3c** bearing a N-CH₂CH₂OH moiety, [3c][TCNQ]. All three salts crystallize in the triclinic system, space group *P1*, with cation and anion in general position (Figure 7). The TCNQ radical anions form almost eclipsed dimers located at the center of the unit cell, with a much shorter plane-to-plane distance (3.14–3.15 Å) than that found above with **3a** and **4a** where the TCNQ adopted a bond-over-ring overlap. On the other hand, the cations interact only sideways with one neighboring cation related by inversion center, with lateral S...S and/or S...Se contacts shown in Figure 7. In the hydroxyl-substituted derivative [3c][TCNQ], we note the presence of an intramolecular O–H...S hydrogen bond with the C=S group of the thiazole core, with the following structural characteristics a H...S distance of 2.618(2) Å and a O–H...S angle of 164.5(2)°, leading here, as in neutral **3c** (Figure 1), to an intramolecular seven-membered motif.

This structural organization common to the three TCNQ salts with **3b**, **3c**, and **4b** strongly differs from that described above with the smaller N-Me derivatives **3a** and **4a**. In the latter, with TCNQ as with TCNQF₄, face-to-face overlap interactions between the dithiolenone (or diselenone) moieties favored a strong overlap between cation radical species. Here, the more sterically demanding –Et (in **3b**, **4b**) or –CH₂CH₂OH (in **3c**) substituents on the nitrogen atom hinder such a face-to-face overlap and limit the interactions to only side contacts, as also confirmed by the calculated $\beta_{\text{HOMO-HOMO}}$ interaction energies, found here in the range 0.036–0.041 eV in the three salts. The temperature dependence of the magnetic interaction of the three salts illustrates this difference. As shown in Figure 8, the salts are

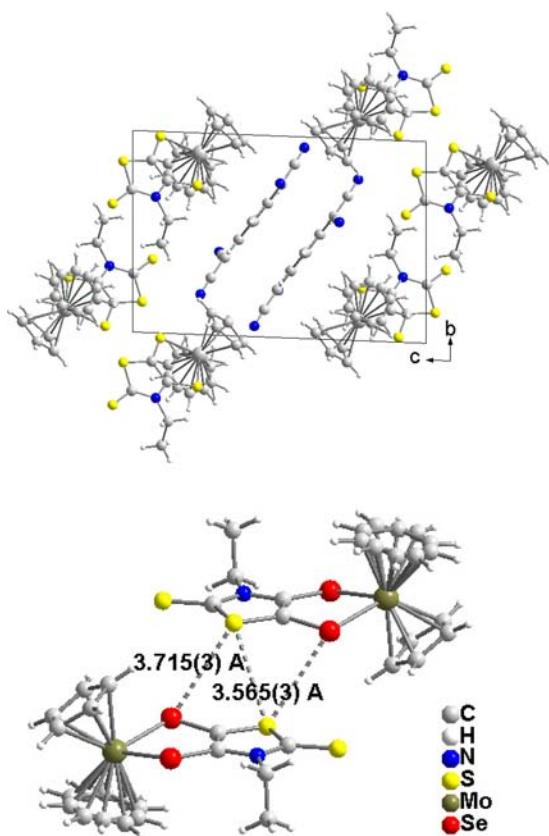


Figure 7. View of the unit cell along the *bc* plane of [3b][TCNQ] (top) and S⋯S and S⋯Se interactions within [4b][TCNQ] (bottom).

not diamagnetic anymore, but the susceptibility goes through a maximum and extrapolates to a singlet state (taking into account a Curie tail) at lower temperatures. Considering that the paired TCNQ radical anion does not contribute because it is strongly dimerized, the susceptibility was very satisfactorily fitted with a Bleaney-Bower singlet–triplet model (eq 1) with x the fraction of Curie-type magnetic defaults and J the magnetic interaction within the cation radical dyads.

$$\chi = \chi_0 + x \cdot \chi_{Curie} + (1 - x) \frac{Ng^2\beta^2}{kT} \frac{1}{3 + \exp(-J/kT)} \quad (1)$$

We found J/k values of $-75.8(2)$, $-53.6(3)$, and $-200.1(8)$ K for [3b][TCNQ], [3c][TCNQ], and [4b][TCNQ], respectively, with Curie tail contributions (x) of 3.9(2), 7.2(4), and 3.3(1)%. The stronger interactions obtained with 4b are attributable to the better overlap between diselenolene complexes.

At variance with the TCNQ salts, the TCNQF₄ salts with 3b, 3c, and 4b are not isostructural, but only [3b][TCNQF₄] and [4b][TCNQF₄], while the hydroxyethyl derivative 3c adopts with TCNQF₄ a different structure. [3b][TCNQF₄] and [4b]-[TCNQF₄] crystallize in the triclinic system, space group $P\bar{1}$, with both cation and anion in general position. Note that strongly disordered solvent molecules (CH₂Cl₂), located close to the center of the unit cell, could not be properly refined. As a consequence, the crystals rapidly decompose and could not be investigated for susceptibility measurements. Within these salts, the radical anion form strongly dimerized chains with different intra- and interdimer overlaps as shown in Figure 9. For the

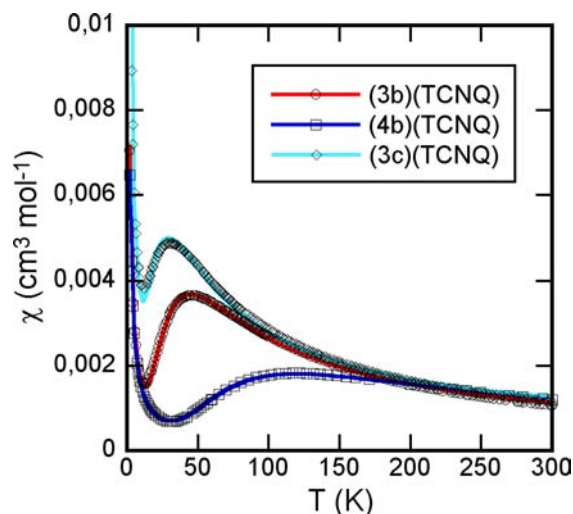


Figure 8. Temperature dependence of the magnetic susceptibility in [3b][TCNQ], [3c][TCNQ], and [4b][TCNQ]. Solid lines are the fits to the singlet–triplet model.

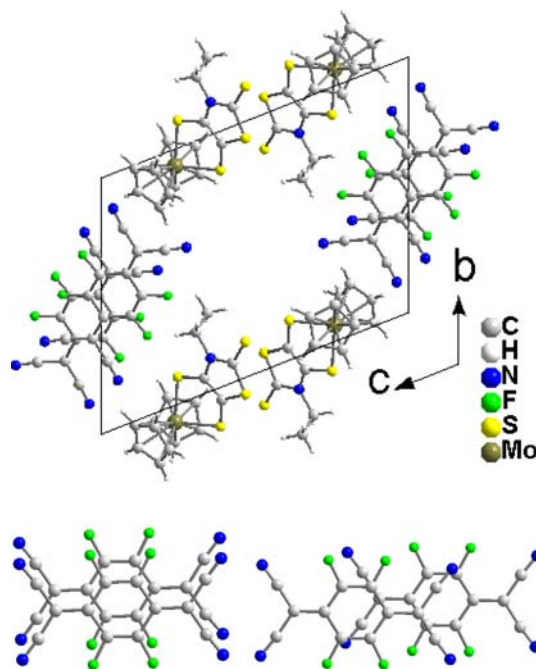


Figure 9. View of the unit cell along the *bc* plane of [3b][TCNQF₄] (top), TCNQF₄ intradimer overlap (bottom left), and TCNQF₄ interdimer overlap (bottom right).

TCNQF₄ dimer, a lateral slip, similar to that observed for the TCNQF₄ salts involving the Me-thiazole core, is observed, while an interdimer longitudinal slip leading to a bond-overbond is observed (Figure 9).

The radical cations are also associated into alternated chains running along *a*, as depicted in Figure 10, with a partial intradimer face-to-face overlap (S⋯S interactions 3.577(3) and 3.138(3) Å for [3b][TCNQF₄] and S⋯S interactions 3.589(2) Å and S⋯Se interactions 3.115(2) Å for [4b][TCNQF₄]) and weaker S⋯S side interactions between dimers (3.535(3) Å for [3b][TCNQF₄] and 3.510(2) Å for [4b][TCNQF₄]). The calculated $\beta_{HOMO-HOMO}$ interaction energies confirm this dimer description, as the intradimer β values are very large (0.66 and 0.79 eV) in [3b][TCNQF₄] and [4b][TCNQF₄], respectively,

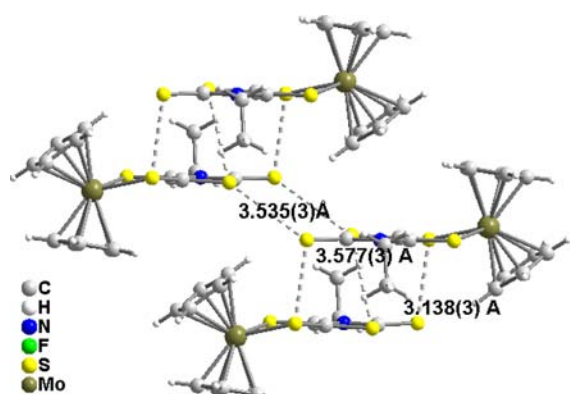


Figure 10. S...S and S...Se interactions within $[3b][TCNQF_4]$.

while the interdimer interactions energies do not exceed 0.04 eV.

Finally, the very last compound described here was obtained with the hydroxyethyl dithiolene derivative **3c** and $TCNQF_4$. It crystallizes in the monoclinic system, space group $P2_1/c$ with both cation and anion in general position in the unit cell. A projection view of the unit cell along the a axis shows the recurrent $TCNQF_4$ dimerization (Figure 11). On the other hand,

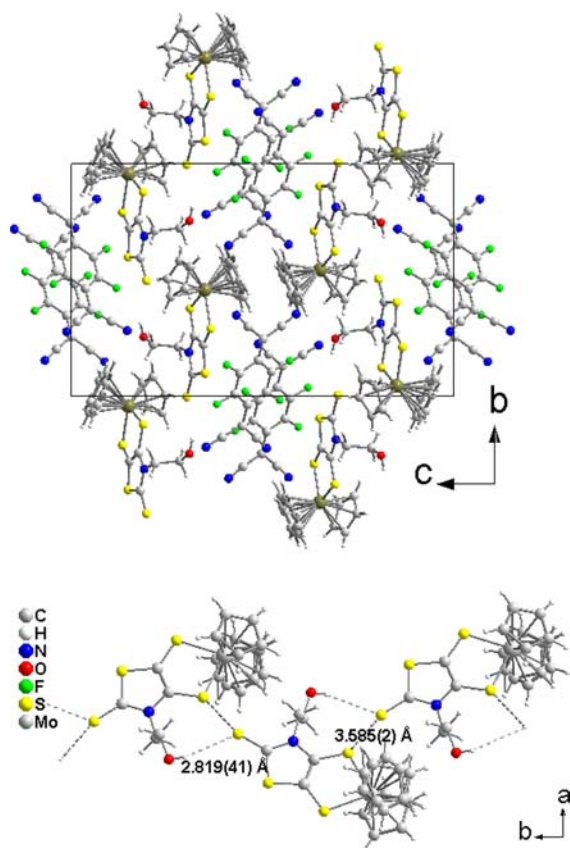


Figure 11. View of the unit cell along the bc plane of $[3c][TCNQF_4]$ (top) and S...S and S...H interactions within $[3c][TCNQF_4]$ (bottom).

the organometallic cation radical adopts an original structure, with the OH group hydrogen-bonded to the sulfur atom of the C=S moiety of a neighboring cation rather than to its own C=S group, as observed in the previous structures described

above, in neutral **3c** as well as in $(3c)(TCNQ)$. As a consequence, the dithiolene moieties of two neighboring cations interact only through one S...S contact involving the very same exocyclic C=S, without any possibility for a stronger face-to-face overlap interaction. This solid state organization is supported by the temperature dependence of the magnetic susceptibility. The strongly dimerized $TCNQF_4$ species are expected to be magnetically silent. As shown in Figure 12, the susceptibility can be fitted with a

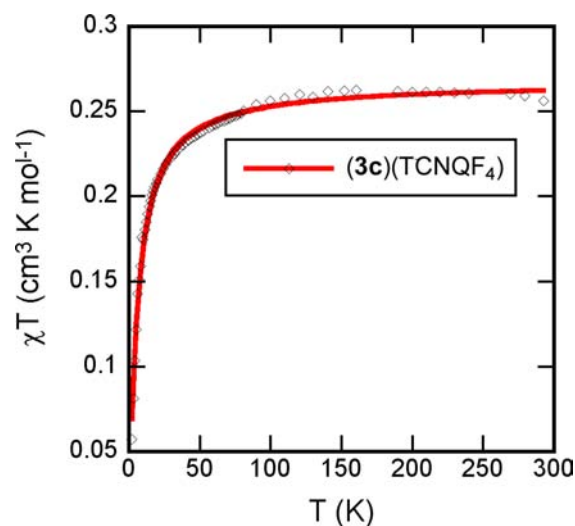


Figure 12. Temperature dependence of the χT product in $[3c][TCNQF_4]$. The solid line is a fit to the Curie–Weiss law (see text).

Curie–Weiss law, with the contribution of one single $S = 1/2$ species ($\approx 75\%$) with $\theta_{CW} = -5.6(1)$ K, confirming the absence of magnetic interactions between cationic species.

Theoretical Insights. When compared with the prototypical $Cp_2Mo(dmit)$ complex, the originality of the $Cp_2Mo(R-thiazdt)$ complexes described here lies in the flexibility offered by the nitrogen substituent as well as in their electron rich character. These two elements combine to favor strong face-to-face overlap interactions in the less sterically hindered complexes ($R = Me$ in **3a**, **4a**), while the larger $R = Et$ or $R = CH_2CH_2OH$ substituents in **3b**, **4b**, and **3c** limit these intermolecular interactions, up to the point where the radical cations are essentially isolated from each other, as in $(3c)(TCNQF_4)$. The electron-rich character of these series was up to now deduced from the electrochemical characterizations of the complexes, which oxidize indeed at a much lower potential than $Cp_2Mo(dmit)$. In order to check this point and to determine to which extent this easier oxidation influences the distribution of the spin density on the whole complex, and incidentally its ability to efficiently overlap in the solid state, we have performed DFT calculations on the simplest $Cp_2Mo(Me-thiazdt)$ complex **3a** and compared them with those previously reported for $Cp_2Mo(dmit)$.⁹ Geometry optimizations (BPW91/LanL2DZ) of $Cp_2Mo(dmit)$ and $Cp_2Mo(Me-thiazdt)$ **3a** in their neutral state yield comparable structures, with a slightly folded MoS_2C_2 metallacycle, the folding angle being respectively 2.4 and 2.6°, Figure 13. The HOMO level of **3a** lies notably higher in energy (by 0.34 eV) than that of $Cp_2Mo(dmit)$ in accordance with electrochemical data (see above). The HOMO of **3a** shows very little metal contribution, while that of $Cp_2Mo(dmit)$ shows none. In the radical cation state, **3a** displays an unchanged conformation of the dithiolene ligand (folding angle 2.3°), and its SOMO (lying at -8.00 eV) and

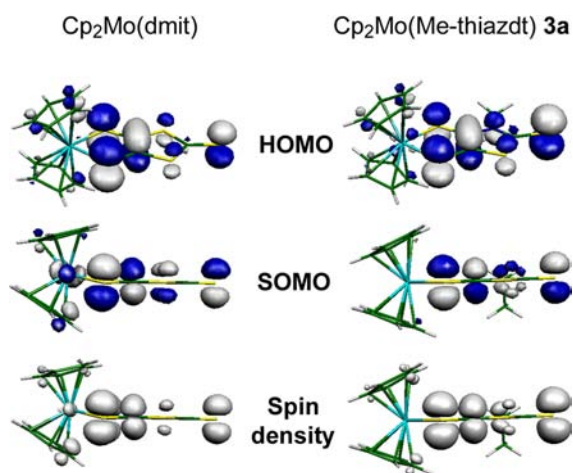


Figure 13. HOMO, SOMO (cutoff 0.04 [e/bohr^3] $^{1/2}$) and spin density (cutoff 0.02 e/bohr^3) of $\text{Cp}_2\text{Mo}(\text{dmit})$ and $[\text{Cp}_2\text{Mo}(\text{dmit})]^{*+}$ (left) and $[\text{Cp}_2\text{Mo}(\text{Me-thiazdt})]$ **3a** and $[\text{3a}]^{*+}$ (right).

spin density are mostly centered on the dithiolene ligand with no contribution of the metal.

On the other hand, for $\text{Cp}_2\text{Mo}(\text{dmit})$, a very flat potential energy surface is found for folding angles between 0 and 15°, differing only by 0.02 eV. In the most stable slightly folded conformation the SOMO and spin density, in $\text{Cp}_2\text{Mo}(\text{dmit})$, display some metal character in addition to the strong dithiolene character. Actually, the folding increases the mixing of the Cp_2Mo and dithiolene frontier orbitals and transfers spin density from the dithiolene to the metal, while the unfolded structure has no metal character.

To conclude, several heteroleptic complexes were prepared and fully characterized. The choice of the substituents ($R = \text{Me}$, Et , EtOH) was performed in order to keep the electron rich ligand character as demonstrated through electrochemical investigations. The oxidation of these new complexes occurs at a lower potential than the oxidation of the dithiole analogues indicating that the most electron rich ligand is the thiazdt over

dmit and thiazds over dsit. Their low oxidation potentials allow the formation of charge transfer salts with TCNQ and TCNQF_4 . The nature of the R substituent, associating steric requirements and hydrogen bonding, modifies the intermolecular arrangements and their associated magnetic behavior. Contrariwise, when the thiazole ring bears the same substituent, the nature of the metallacycle, dithiolene vs diselenolene, does not modify the organization of the oxidized species in the solid state, but the presence of the selenium atoms strengthens the intermolecular interactions. For all these oxidized complexes, the degree of flexibility observed in the metallacycle ring is not correlated with the degree of charge transfer, as in two cases the oxidized species are less distorted than the neutral one, but more with the packing organization of the molecules in the solid state, a direct consequence of the very flat potential energy surface upon metallacycle folding, as confirmed by DFT calculations on these open shell, formally d^1 , organometallic species.

EXPERIMENTAL SECTION

The thiazoline-2-thione **1a–c** and **2a–b** were synthesized according to the literature procedure.^{11–14} All air-sensitive reactions were carried out under argon atmosphere. Melting points were measured on a Kofler hot-stage apparatus and are uncorrected. ^1H NMR and ^{13}C NMR spectra were recorded on a Bruker AV300III spectrometer using $(\text{CD}_3)_2\text{SO}$ as solvent. Chemical shifts are quoted in parts per million (ppm) referenced to tetramethylsilane. Mass spectra were recorded with Varian MAT 311 instrument by the Centre Régional de Mesures Physiques de l'Ouest, Rennes. Elemental analysis were performed at the Centre Régional de Mesures Physiques de l'Ouest, Rennes. Tetrahydrofuran was distilled from sodium-benzophenone. Column chromatography was performed using silica gel Merck 60 (70–260 mesh). Cyclic voltammetry were carried out on a 10^{-3} M solution of the complex in CH_2Cl_2 , containing 0.1 M $n\text{Bu}_4\text{NPF}_6$ as supporting electrolyte. Voltammograms were recorded at 0.1 V s^{-1} on a platinum disk electrode ($A = 1 \text{ mm}^2$). The potentials were measured versus Saturated Calomel Electrode.

Synthesis of $[\text{Cp}_2\text{Mo}(\text{R-thiazdt})]$ **3a–c and $[\text{Cp}_2\text{Mo}(\text{R-thiazds})]$ **4a–b**.** To a solution of thiazoline-2-thione (0.9 mmol, 270 mg for **1a**, 280 mg for **1b**, 300 mg for **1c**, 350 mg for **2a**, and 370 mg for **2b**) in 5 mL of dry MeOH under inert atmosphere was added a solution of

Table 4. Crystallographic Data for the Neutral Complexes $\text{Cp}_2\text{Mo}(\text{R-thiazdt})$ **3a–c** and **4a–b** $\text{Cp}_2\text{Mo}(\text{R-thiazds})$

compound	3a	3b	3c	4a	4b
formula	$\text{C}_{14}\text{H}_{13}\text{MoNS}_4$	$\text{C}_{15}\text{H}_{15}\text{MoNS}_4$	$\text{C}_{15}\text{H}_{15}\text{MoNOS}_4$	$\text{C}_{14}\text{H}_{13}\text{MoNS}_2\text{Se}_2$	$\text{C}_{15}\text{H}_{15}\text{MoNS}_2\text{Se}_2$
FW ($\text{g}\cdot\text{mol}^{-1}$)	419.43	433.46	449.5	513.23	527.26
crystal system	monoclinic	monoclinic	monoclinic	monoclinic	triclinic
space group	$P2_1/c$	$P2_1/n$	$P2_1/c$	$P2_1/c$	$P-1$
a (Å)	10.6826(2)	11.3067(14)	10.7409(2)	10.8880(16)	6.8982(3)
b (Å)	10.6630(2)	12.0229(15)	11.2682(2)	10.7812(15)	11.1040(5)
c (Å)	13.3238(3)	12.4471(15)	13.5349(2)	13.3725(18)	11.2821(5)
α (°)	90	90	90	90	98.754(2)
β (°)	97.345(1)	108.624(4)	97.538(1)	98.071(5)	107.099(2)
γ (°)	90	90	90	90	96.239(2)
V (Å ³)	1505.24(5)	1603.4(3)	1623.98(5)	1554.2(4)	805.52(6)
T (K)	150(2)	150(2)	150(2)	150(2)	150(2)
Z	4	4	4	4	2
D_{calc} ($\text{g}\cdot\text{cm}^{-3}$)	1.851	1.796	1.838	2.193	2.174
μ (mm^{-1})	1.413	1.330	1.321	5.784	5.583
total refls.	13435	11771	13910	23149	3534
unique refls. (R_{int})	3444 (0.0291)	3624 (0.0438)	3718 (0.0243)	3539(0.0367)	3534(0)
unique refls. ($I > 2\sigma(I)$)	3092	3254	3400	3263	3150
R_1, wR_2	0.0259, 0.0576	0.0262, 0.0593	0.0222, 0.0529	0.021, 0.0508	0.0294, 0.0916
R_1, wR_2 (all data)	0.030, 0.0608	0.0303, 0.0611	0.0254, 0.0548	0.0242, 0.0524	0.0362, 0.1036
GoF	1.035	1.033	1.036	1.031	1.202

Table 5. Crystallographic Data for the TCNQ/Cp₂Mo(R-thiazdt) and TCNQ/Cp₂Mo(R-thiazds) Complexes

compound	[3a][TCNQ]	[4a][TCNQ]	[3b][TCNQ]	[3c][TCNQ]	[4b][TCNQ]
formula	C ₂₆ H ₁₇ MoN ₅ S ₄	C ₂₆ H ₁₇ MoN ₅ S ₂ Se ₂	C ₂₇ H ₁₉ MoN ₅ S ₄	C ₂₇ H ₁₉ MoN ₅ OS ₄	C ₂₇ H ₁₉ MoN ₅ S ₂ Se ₂
FW (g·mol ⁻¹)	623.63	717.43	637.65	653.65	731.45
crystal system	triclinic	triclinic	triclinic	triclinic	triclinic
space group	P $\bar{1}$	P $\bar{1}$	P $\bar{1}$	P $\bar{1}$	P $\bar{1}$
a (Å)	7.5847(3)	7.6898(2)	7.8560(8)	7.8882(2)	7.9167(3)
b (Å)	12.8363(4)	12.7868(4)	10.9798(13)	10.9990(3)	11.0042(5)
c (Å)	13.3970(5)	13.3717(4)	15.4149(18)	15.3320(4)	15.6348(7)
α (°)	74.095(2)	73.896(1)	87.393(5)	87.625(1)	86.582(2)
β (°)	85.672(2)	84.307(1)	88.209(5)	88.530(1)	87.829(2)
γ (°)	86.179(2)	86.008(1)	73.987(5)	73.203(1)	73.733(2)
V (Å ³)	1249.38(8)	1255.77(6)	1276.5(2)	1272.26(6)	1304.88(10)
T (K)	150(2)	150(2)	150(2)	150(2)	296(2)
Z	2	2	2	2	2
D _{calc} (g·cm ⁻³)	1.658	1.897	1.659	1.706	1.862
μ (mm ⁻¹)	0.886	3.614	0.869	0.877	3.480
total refls.	17255	18142	19085	17774	21827
unique refls. (R _{int})	5691(0.0404)	5674(0.0409)	5703 (0.0465)	5732(0.0387)	5926(0.0598)
unique refls. (I > 2 σ (I))	4799	4899	4997	4871	3956
R ₁ , wR ₂	0.0388, 0.085	0.0313, 0.0686	0.033, 0.0719	0.0394, 0.0854	0.0432, 0.0821
R ₁ , wR ₂ (all data)	0.0495, 0.091	0.039, 0.0714	0.0397, 0.0754	0.049, 0.090	0.0809, 0.0953
GoF	0.872	1.038	1.031	1.05	1.047

Table 6. Crystallographic Data for the TCNQF₄/Cp₂Mo(R-thiazdt) and TCNQF₄/Cp₂Mo(R-thiazds) Complexes

compound	[3a][TCNQF ₄]	[4a][TCNQF ₄]	[3b][TCNQF ₄]	[4b][TCNQF ₄]	[3c][TCNQF ₄]
formula	C ₂₆ H ₁₃ F ₄ MoN ₅ S ₄	C ₂₆ H ₁₃ F ₄ MoN ₅ S ₂ Se ₂	C ₂₇ H ₁₅ F ₄ MoN ₅ S ₄	C ₂₇ H ₁₅ F ₄ MoN ₅ S ₂ Se ₂	C ₂₇ H ₁₅ F ₄ MoN ₅ OS ₄
FW (g·mol ⁻¹)	695.59	789.39	709.62	803.42	725.62
crystal system	monoclinic	monoclinic	triclinic	triclinic	monoclinic
space group	C2/c	C2/c	P $\bar{1}$	P $\bar{1}$	P 2 ₁ /n
a (Å)	17.0484(11)	16.8122(6)	7.5998(3)	7.6315(2)	8.3701(2)
b (Å)	25.4809(16)	25.6597(9)	13.3602(7)	13.2522(4)	13.8913(4)
c (Å)	13.8577(7)	14.0170(4)	16.6712(8)	16.7904(5)	22.9983(7)
α (°)	90	90	109.574(2)	109.449(1)	90
β (°)	118.125(2)	117.263(1)	93.545(2)	93.931(1)	90.350(1)
γ (°)	90	90	105.767(2)	105.315(1)	90
V (Å ³)	5309.1(5)	5375.1(3)	1512.91(12)	1521.29(8)	2674.00(13)
T (K)	150(2)	150(2)	150(2)	150(2)	150(2)
Z	8	8	2	2	4
D _{calc} (g·cm ⁻³)	1.741	1.951	1.558	1.754	1.802
μ (mm ⁻¹)	0.865	3.408	0.760	3.012	0.865
total refls.	22584	22736	22353	24220	23656
unique refls. (R _{int})	6065 (0.0479)	6108(0.034)	6770(0.0444)	6756(0.0422)	6088(0.0425)
unique refls. (I > 2 σ (I))	5134	4874	5615	5126	5207
R ₁ , wR ₂	0.0314, 0.0814	0.0311, 0.0721	0.0349, 0.0851	0.0418, 0.0996	0.0319, 0.0741
R ₁ , wR ₂ (all data)	0.0386, 0.0848	0.0457, 0.0755	0.0445, 0.0883	0.0608, 0.1061	0.0393, 0.0785
GoF	1.052	1.102	1.028	1.064	1.043

NaOMe (7.5 mmol, 7.5 mL of 1 M solution in MeOH). The reaction mixture was stirred for 1 h at room temperature, and a solution of Cp₂MoCl₂ (0.9 mmol, 260 mg) in 20 mL of THF was added. The reaction mixture was refluxed 4 h. The solvent was removed *in vacuo*, and 15 mL of water was added. The precipitate was filtered off, washed with water and EtOH, and recrystallized in chloroform.

3a [Cp₂Mo(Me-thiazdt)] black crystals, yield 63%, mp >400 °C, ¹H NMR (300 MHz) δ 3.55 (s, 3H, CH₃), 5.58 (s, 10H, 2 Cp); ¹³C NMR (75 MHz) δ 35.0 (CH₃), 98.8 (Cp), 121.8 (=C), 146.9 (=C), 184.6 (C=S); UV-vis (CH₃CN) λ (nm) (ϵ [L·mol⁻¹ cm⁻¹]) 263 (11100), 395 (6316); Anal. Calcd for C₁₄H₁₃MoNS₄: C, 40.09; H 3.12; N, 3.34; S, 30.58. Found: C, 40.24; H 3.21; N, 3.30; S, 30.38.

3b [Cp₂Mo(Et-thiazdt)] black crystals, yield 68%, mp >400 °C, ¹H NMR (300 MHz) δ 1.19 (t, 3H, CH₃), 4.15 (q, 2H, CH₂N), 5.53 (s, 10H, 2 Cp); ¹³C NMR (75 MHz) δ 11.8 (CH₃), 42.0 (CH₂), 98.2 (Cp), 121.0 (=C), 145.7 (=C), 183.0 (C=S); UV-vis (CH₃CN) λ (nm) (ϵ [L·mol⁻¹ cm⁻¹]) 261 (13700), 395 (8040); HRMS calcd for C₁₅H₁₅MoNS₄: 434.91359. Found: 434.9135.

3c [Cp₂Mo(EtOH-thiazdt)] black crystals, yield 63%, mp >250 °C, ¹H NMR (300 MHz) δ 3.58 (m, 2H, CH₂OH, J = 6.3 Hz), 4.18 (t, 2H, NCH₂, J = 7.2 Hz), 4.93 (t, 1H, OH, J = 5.7 Hz), 5.52 (s, 10H, 2Cp). ¹³C NMR (75 MHz) δ 49.4 (CH₂N), 56.7 (CH₂O), 98.8 (Cp), 122.1 (=C), 147.0 (=C), 185.0 (C=S); UV-vis (CH₃CN) λ (nm) (ϵ [L·mol⁻¹ cm⁻¹]) 263 (13530), 400 (7750); HRMS (ESI) calcd for C₁₅H₁₅MoNOS₄: 450.9091. Found: 450.9095; Anal. Calcd for

$C_{15}H_{15}MoNO_4$: C, 40.26; H 2.93; N, 3.13; S, 28.66. Found: C, 40.03; H 3.41; N, 3.02; S, 28.57.

4a [$Cp_2Mo(Me-thiazds)$] black crystals, yield 90%, mp >400 °C, 1H NMR (300 MHz) δ = 3.60 (s, 3H, CH_3), 5.57 (s, 10H, 2 Cp); ^{13}C NMR (75 MHz) δ = 37.0 (CH_3), 96.6 (Cp), 107.1 (=C), 137.9 (=C), 187.6 (C=S); UV-vis (CH_3CN) λ (nm) (ϵ [$L \cdot mol^{-1} cm^{-1}$]) 268 (12790), 388 (7100); Anal. Calcd for $C_{14}H_{13}MoNS_2Se_2$: C, 32.76; H 2.55; N, 2.73; S, 12.49. Found: C, 32.75; H 2.60; N, 2.75; S, 12.82.

4b [$Cp_2Mo(Et-thiazds)$] black crystals, yield 76%, mp >400 °C, 1H NMR (300 MHz) δ 1.28 (t, 3H, CH_3), 4.26 (q, 2H, CH_2N), 5.60 (s, 10H, 2 Cp); ^{13}C NMR (75 MHz) δ 12.7 (CH_3), 45.0 (CH_2), 96.6 (Cp), 107.7 (=C), 137.1 (=C), 187.1 (C=S); UV-vis (CH_3CN) λ (nm) (ϵ [$L \cdot mol^{-1} cm^{-1}$]) 269 (19800), 391 (10197); HRMS calcd for $C_{14}H_{13}MoNS_2Se_2$: 530.80249. Found: 530.8028.

Preparation of TCNQ and TCNQF₄ Salts. To a hot solution of neutral Mo complex (0.03 mmol) in 15 mL of CH_2Cl_2 was added a hot solution of TCNQ or TCNQF₄ (0.03 mmol) in 15 mL of CH_3CN . The reaction mixture was refluxed 5 min, and the solvent was slowly evaporated to afford dark violet crystals.

Crystallography. Data were collected on an APEX II Bruker AXS diffractometer with graphite-monochromated Mo- $K\alpha$ radiation (λ = 0.71073 Å). The structure were solved by direct methods using the SIR97 program³⁰ and then refined with full-matrix least-squares methods based on F^2 (SHELXL-97)³¹ with the aid of the WINGX program.³² For [3a][TCNQF₄], [3b][TCNQF₄], [4a][TCNQF₄], and [4b][TCNQF₄], the contribution of the disordered solvents to the calculated structure factors was estimated following the BYPASS algorithm,³³ implemented as the SQUEEZE option in PLATON.³⁴ A new data set, free of solvent contribution, was then used in the final refinement. For all structures, all non-hydrogen atoms were refined with anisotropic atomic displacement parameters. Except for one linked hydrogen atom (H17), for 3c and [3c][TCNQF₄], that was introduced in the structural model through Fourier difference maps analysis, H atoms were finally included in their calculated positions. Details of the final refinements are given in Tables 4–6 for all compounds.

Theoretical Calculations. Calculations of the intermolecular β overlap interactions energies were performed with the extended Hückel method.³⁵ A modified Wollberg-Helmholtz formula was used to calculate the $H_{\mu\nu}$ nondiagonal values.³⁶ Double- ζ orbitals were used for all atoms except hydrogen. The Caesar suite of programs was used to perform these calculations.³⁷ DFT calculations were performed with Gaussian09,³⁸ as described for $Cp_2Mo(dmit)$,⁹ in reference using the BPW91 functional with Becke gradient correction for exchange³⁹ and Perdew–Wang corrections for correlation.⁴⁰ A double- ζ basis with electron core pseudopotentials (LANL2DZ) was used.⁴¹ Initial geometries were derived from the X-ray crystallographic studies. Figures were generated with MOLEKEL 4.3.⁴²

■ ASSOCIATED CONTENT

● Supporting Information

A crystallographic file in CIF format is provided. This material is available free of charge via the Internet at <http://pubs.acs.org>.

■ AUTHOR INFORMATION

Corresponding Author

*E-mail: dominique.lorcy@univ-rennes1.fr.

Notes

The authors declare no competing financial interest.

■ ACKNOWLEDGMENTS

We thank the CINES (Montpellier) for allocation of computing time.

■ REFERENCES

(1) Taylor, A. J.; Davies, E. S.; Weinstein, J. A.; Sazanovich, I. V.; Bouganov, O. V.; Tikhomirov, S. A.; Towrie, M.; McMaster, J.; Garner, C. D. *Inorg. Chem.* **2012**, *51*, 13181–13194.

(2) (a) Collison, D.; Garner, C. D.; Joule, J. A. *Chem. Soc. Rev.* **1996**, 25–32. (b) Hine, F. J.; Taylor, A. J.; Garner, C. D. *Coord. Chem. Rev.* **2010**, *254*, 1570–1579.

(3) Davies, E. S.; Beddoes, R. L.; Collison, D.; Dinsmore, A.; Docrat, A.; Joule, J. A.; Wilson, C. R.; Garner, C. D. *J. Chem. Soc., Dalton Trans.* **1997**, 3985–3996.

(4) (a) Kaiwar, S. P.; Hsu, J. K.; Vodacek, A.; Yap, G.; Liable-Sands, L. M.; Rheingold, A. L.; Pilato, R. S. *Inorg. Chem.* **1997**, *36*, 2406–2412. (b) Hsu, J. K.; Bonangelino, C. J.; Kaiwar, S. P.; Boggs, C. M.; Fetting, J. C.; Pilato, R. S. *Inorg. Chem.* **1996**, *35*, 4743–4751.

(5) Fourmigué, M. *Acc. Chem. Res.* **2004**, *37*, 179–186.

(6) Fourmigué, M. *Coord. Chem. Rev.* **1998**, *178–180*, 823–864.

(7) Fourmigué, M.; Lenoir, C.; Coulon, C.; Guyon, F.; Amaudrut, J. *Inorg. Chem.* **1995**, *34*, 4979–4985.

(8) Clérac, R.; Fourmigué, M.; Coulon, C. *J. Solid. State Chem.* **2001**, *159*, 413–419.

(9) Domercq, B.; Coulon, C.; Fourmigué, M. *Inorg. Chem.* **2001**, *40*, 371–378.

(10) Fourmigué, M.; Domercq, B.; Jourdain, I. V.; Molinié, P.; Guyon, F.; Amaudrut, J. *Chem.—Eur. J.* **1998**, *4*, 1714–1723.

(11) Eid, S.; Guerro, M.; Lorcy, D. *Tetrahedron Lett.* **2006**, *47*, 8333–8336.

(12) (a) Aragoni, M. C.; Arca, M.; Devillanova, F. A.; Isaia, F.; Lippolis, V.; Mancini, A.; Pala, L.; Slawin, A. M. Z.; Woollins, J. D. *Inorg. Chem.* **2005**, *44*, 9610. (b) Eid, S.; Fourmigué, M.; Roisnel, T.; Lorcy, D. *Inorg. Chem.* **2007**, *46*, 10647–10654.

(13) (a) Tenn, N.; Bellec, N.; Jeannin, O.; Piekara-Sady, L.; Auban-Senzier, P.; Íñiguez, J.; Canadell, E.; Lorcy, D. *J. Am. Chem. Soc.* **2009**, *131*, 16961–16967. (b) Yzambart, G.; Bellec, N.; Ghassan, N.; Jeannin, O.; Roisnel, T.; Fourmigué, M.; Auban-Senzier, P.; Íñiguez, J.; Canadell, E.; Lorcy, D. *J. Am. Chem. Soc.* **2012**, *134*, 17138–17148.

(14) Eid, S.; Roisnel, T.; Lorcy, D. *J. Organomet. Chem.* **2008**, *693*, 2755–2760.

(15) Pintus, A.; Aragoni, M. C.; Bellec, N.; Devillanova, F. A.; Lorcy, D.; Isaia, F.; Lippolis, V.; Randall, R. A. M.; Roisnel, T.; Slawin, A. M. Z.; Woollins, J. D.; Arca, M. *Eur. J. Inorg. Chem.* **2012**, 3577–3594.

(16) Steiner, T. *Angew. Chem., Int. Ed.* **2002**, *41*, 48–76.

(17) Whalley, A. L.; Blake, A. J.; Collison, D.; Davies, E. S.; Disley, H. J.; Helliwell, M.; Mabbs, F. E.; McMaster, J.; Wilson, C.; Garner, C. D. *Dalton Trans.* **2011**, *40*, 10457–10472.

(18) Green, M. L. H.; Lindsell, W. E. *J. Chem. Soc. A* **1967**, 1455–1458.

(19) Kistenmacher, T. J.; Emge, T. J.; Bloch, A. N.; Cowan, D. O. *Acta Crystallogr., Sect. B: Struct. Crystallogr. Cryst. Chem.* **1982**, *B38*, 1193–1199.

(20) Chappell, J. S.; Bloch, A. N.; Bryden, W. A.; Maxfield, M.; Poehler, T. O.; Cowan, D. O. *J. Am. Chem. Soc.* **1981**, *103*, 2442–2443.

(21) (a) Torrance, J. B.; Vazquez, J. E.; Mayerle, J. J.; Lee, V. Y. *Phys. Rev. Lett.* **1981**, *46*, 253–257. (b) Saito, G.; Ferraris, J. P. *Bull. Chem. Soc. Jpn.* **1980**, *53*, 2141–2145.

(22) Miller, J. S.; Zhang, J. H.; Reiff, W. M. *Inorg. Chem.* **1987**, *26*, 600–608.

(23) Long, R. E.; Sparks, R. A.; Trueblood, K. N. *Acta Crystallogr.* **1965**, *18*, 932–939.

(24) Giraldo, A.; Pecile, C. *Spectrochim. Acta, Part A* **1973**, *29A*, 1859–1878.

(25) Konno, M.; Saito, Y. *Acta Crystallogr., Sect. B: Struct. Crystallogr. Cryst. Chem.* **1974**, *B30*, 1294–1299.

(26) Emge, T. J.; Maxfield, M.; Cowan, D. O.; Kistenmacher, T. J. *Mol. Cryst. Liq. Cryst.* **1981**, *65*, 161–178.

(27) Murata, T.; Saito, G.; Nishimura, K.; Enomoto, Y.; Honda, G.; Shimizu, Y.; Matsui, S.; Sakata, M.; Drozdova, O. O.; Yakushi, K. *Bull. Chem. Soc. Jpn.* **2008**, *81*, 331–344.

(28) Kistenmacher, T. J.; Phillips, T. E.; Cowan, D. O. *Acta Crystallogr., Sect. B: Struct. Crystallogr. Cryst. Chem.* **1974**, *B30*, 763–768.

(29) Such $Cp \cdots Cp$ interactions have been shown to play a prominent role in the magnetic behavior of heteroleptic complexes such as

[CpNi(dithiolene)][•] characterized with a sizable spin density on the Cp ring in the absence of dithiolene/dithiolene interactions. See for example: (a) Reinheimer, E. W.; Olejniczak, I.; Łapiński, A.; Świetlik, R.; Jeannin, O.; Fourmigué, M. *Inorg. Chem.* **2010**, *49*, 9777–9787. (b) Fourmigué, M.; Cauchy, T.; Nomura, M. *CrystEngComm* **2009**, *11*, 1491–1501. (c) Nomura, M.; Cauchy, T.; Geoffroy, M.; Adkine, P.; Fourmigué, M. *Inorg. Chem.* **2006**, *45*, 8194–8204.

(30) Altomare, A.; Burla, M. C.; Camalli, M.; Cascarano, G.; Giacovazzo, C.; Guagliardi, A.; Moliterni, A. G. G.; Polidori, G.; Spagna, R. *J. Appl. Crystallogr.* **1999**, *32*, 115–119.

(31) Sheldrick, G. M. *Acta Crystallogr., Sect. A: Found. Crystallogr.* **2008**, *A64*, 112–122.

(32) Farrugia, L. J. *J. Appl. Crystallogr.* **1999**, *32*, 837–838.

(33) v.d. Sluis, P.; Spek, A. L. *Acta Crystallogr., Sect. A: Found. Crystallogr.* **1990**, *A46*, 194–201.

(34) Spek, A. L. *J. Appl. Crystallogr.* **2003**, *36*, 7–13.

(35) Hoffmann, R. *J. Chem. Phys.* **1963**, *39*, 1397–1412.

(36) Ammeter, J. H.; Bürgi, H. B.; Thibeault, J.; Hoffmann, R. *J. Am. Chem. Soc.* **1978**, *100*, 3686–3692.

(37) Ren, J.; Liang, W.; Whangbo, M.-H. *Crystal and Electronic Structure Analysis Using CAESAR*; North Carolina State University: 1998.

(38) Frisch, M. J.; Trucks, G. W.; Schlegel, H. B.; Scuseria, G. E.; Robb, M. A.; Cheeseman, J. R.; Scalmani, G.; Barone, V.; Mennucci, B.; Petersson, G. A.; Nakatsuji, H.; Caricato, M.; Li, X.; Hratchian, H. P.; Izmaylov, A. F.; Bloino, J.; Zheng, G.; Sonnenberg, J. L.; Hada, M.; Ehara, M.; Toyota, K.; Fukuda, R.; Hasegawa, J.; Ishida, M.; Nakajima, T.; Honda, Y.; Kitao, O.; Nakai, H.; Vreven, T.; Montgomery, J. A., Jr.; Peralta, J. E.; Ogliaro, F.; Bearpark, M.; Heyd, J. J.; Brothers, E.; Kudin, K. N.; Staroverov, V. N.; Kobayashi, R.; Normand, J.; Raghavachari, K.; Rendell, A.; Burant, J. C.; Iyengar, S. S.; Tomasi, J.; Cossi, M.; Rega, N.; Millam, N. J.; Klene, M.; Knox, J. E.; Cross, J. B.; Bakken, V.; Adamo, C.; Jaramillo, J.; Gomperts, R.; Stratmann, R. E.; Yazyev, O.; Austin, A. J.; Cammi, R.; Pomelli, C.; Ochterski, J. W.; Martin, R. L.; Morokuma, K.; Zakrzewski, V. G.; Voth, G. A.; Salvador, P.; Dannenberg, J. J.; Dapprich, S.; Daniels, A. D.; Farkas, Ö.; Foresman, J. B.; Ortiz, J. V.; Cioslowski, J.; Fox, D. J. *Gaussian 09, Revision A.02*; Gaussian, Inc.: Wallingford, CT, 2009.

(39) (a) Becke, A. D. *Phys. Rev.* **1986**, *B33*, 8822. (b) Becke, A. D. *ACS Symp. Ser.* **1989**, *394*, 165. (c) Becke, A. D. *Int. J. Quantum Chem.* **1989**, Symp. No. 23, 599.

(40) Perdew, J. P.; Wang, Y. *Phys. Rev.* **1992**, *B45*, 13244.

(41) (a) Dunning, T. H. Jr.; Hay, P. J. In *Modern Theoretical Chemistry*; Schaefer, H. F., III, Ed.; Plenum Press: New York, 1976; Vol. 1. (b) Hay, P. J.; Wadt, W. R. *J. Chem. Phys.* **1985**, *82*, 270. (c) Hay, P. J.; Wadt, W. R. *J. Chem. Phys.* **1985**, *82*, 284. (d) Hay, P. J.; Wadt, W. R. *J. Chem. Phys.* **1985**, *82*, 299.

(42) Flükiger, H. P.; Lüthi, S.; Portmann, S.; Weber, J. *MOLEKEL 4.3*; Swiss National Supercomputing Centre CSCS: Manno, Switzerland, 2000.